Available online at www.sciencedirect.com
ScienceDirect
Combustion and Flame 154 (2008) 82–95
Combustion and Flame
www.elsevier.com/locate/combustflame

Propagating edge-flame response to multiple stoichiometry gradients

Stanislav Kostka Jr., William F. Carnell Jr., Michael W. Renfro *

Department of Mechanical Engineering, 191 Auditorium Rd, U-3139, University of Connecticut, Storrs, CT 06269, USA

Received 3 July 2007; received in revised form 7 December 2007; accepted 14 January 2008

Available online 21 February 2008

Abstract

A five-slot contoured nozzle burner was used to create multiple lifted partially premixed flames in close proximity. The burner permits the stoichiometry gradient below each edge flame and the separation distance between stabilization points of the flames to be separately controlled. In previous work, we showed that edge-flame interactions lead to a bifurcation in the flame stabilization, where the liftoff height of neighboring edge flames differs even in symmetric flow fields. As the composition gradient below each flame is decreased, the edge flames broaden. Flow around the edge flames leads to an aerodynamic interaction, where upstream conditions below one flame are modified by the neighboring flame. These interactions cause a liftoff height difference between the two flames. Further reduction of stoichiometry gradient causes the neighboring flames to merge and approach the structure of a single premixed flame. In this work, the equivalence ratio gradient and separation distance between stoichiometric points were varied by controlling the burner slot equivalence ratios, so that these interactions could be studied in greater detail. Rayleigh scattering was used to measure flame curvature and calculate local stoichiometry gradients below each flame stabilization point. Planar laser-induced fluorescence signals of hydroxyl and formaldehyde were measured to provide qualitative comparisons of relative reaction rates between flames. Neighboring edge flames were found to behave based solely on local conditions below each flame. Only aerodynamic interactions were observed and no chemical or thermal interactions, caused by heat or radical transport between flames, were observed. The bifurcated flame response can be described simply from the effects that flow around the flame structure has on local velocities and scalar dissipation rates.

Keywords: Lifted edge flames; Rayleigh scattering; Stoichiometry gradient; Formaldehyde PLIF; Hydroxyl PLIF

1. Introduction

The propagation and liftoff behavior of single laminar edge flames has been researched extensively in an attempt to characterize and model the behavior of edge flames in partially premixed flows. The edge-flame structure can result in a triple flame when the local stoichiometry includes both rich and lean regions around the stabilization point that occurs near stoichiometric conditions. In turbulent flows, partially premixed mixtures of fuel and air can be present with a range of local scalar dissipation rates and length scales, causing numerous stoichiometric crossings and rich and lean regions within a few millimeters of each other [1]. These stoichiometric crossings within

* Corresponding author. Fax: +1 (860) 486 5088.
E-mail address: renfro@engr.uconn.edu (M.W. Renfro).

0010-2180/$ – see front matter
doi:10.1016/j.combustflame.2008.01.004

close proximity can yield multiple stabilization points and multiple neighboring propagating edge flames, which may interact with each other. Wason et al. [2] have recently shown that interactions between neighboring triple-flame structures can yield a bifurcated flame response where the two interacting edge flames stabilize at different heights even in symmetric flow fields. This paper focuses on these interactions of lifted neighboring edge flames and examines in detail the physical origin of the bifurcation, using optical diagnostics to measure the conditions below both edge flames. Quantitative information on the scalar dissipation rates leading to edge-flame bifurcation will aid in the development of models for flame propagation in turbulent environments, where flame interactions may take place and alter overall flame stability. In addition, flame fronts within the leading edge of each experimental configuration were measured using planar laser-induced fluorescence (PLIF) to determine hydroxyl and formaldehyde distributions. These images were used to estimate relative HCO formation rates, as demonstrated by Paul and Najm [3]. Comparisons are made between these measurements to determine the levels of both aerodynamic and chemical interactions between the bifurcated neighboring edge flames.

2. Background

The triple-flame structure, which was first observed by Philips [4], can be created under partially premixed conditions with a stoichiometric crossing and both lean and rich regions, where the base of the flame stabilizes near the stoichiometric point. The triple-flame structure consists of three branches, a rich premixed branch, a lean premixed branch, and a characteristic trailing diffusion branch [4,5], as depicted in Fig. 1, where mixing between separate fuel and air flows creates a stoichiometry gradient with a single stoichiometric point. Experimental studies performed by Philips [4] on laminar edge flames found that the propagation speeds could be as much as five times the laminar burning velocity. This observation led to further interest in triple flames and detailed studies by, for example, Kioni et al. [6,7], Santoro et al. [8], and Kim et al. [9]. Kioni et al. [6] and Kim et al. [9] used a slot burner to determine the effects of scalar dissipation on the velocity of the edge flame structure, while Santoro et al. [8] used a counterflow diffusion flame to study scaling of flame stabilization and velocity on the strain rate.

Early numerical analysis of the triple flame formed in a nonuniform mixture [10–13] studied propagation velocity behavior, but did not incorporate heat release from the flame, allowing simplification of analysis.

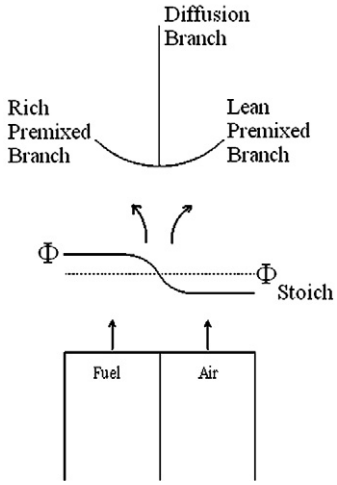

Fig. 1. Lifted edge flame showing characteristic three-branch structure.

Ruetsch et al. [14], however, incorporated heat release and showed that velocity divergence around the edge-flame structure caused by heat release resulted in a deceleration of flow leading up to the flame edge, as observed by Philips [4]. Kioni et al. [7] and Kim et al. [9] verified the observation of Philips [4] that the velocity of the flow leading up to the edge-flame front decreased to approximately the laminar flame speed, using particle imaging velocimetry (PIV) measurements of the flames. This 2-D velocity divergence, shown in Fig. 1, is a critical part of edge-flame stability and enables the edge-flame structure to propagate in faster flows than a 1-D planar premixed flame. Ruetsch et al. [14] found that the propagation velocity is proportional to the laminar stoichiometric burning velocity and the square root of the density ratio between unburnt and burnt mixtures. Dold [11] further showed that the triple-flame propagation speed depends inversely on the transverse mixture fraction gradient and must be above the maximum adiabatic laminar flame speed of the system; this effect of concentration gradient below a single edge flame has led to many experimental studies [2,6,7,15,16].

A very important observation for single-edge-flame behavior is that the edge-flame curvature measured at the local flame front changes depending on the upstream concentration gradient [15]. Fig. 2 depicts two triple flames with different upstream scalar dissipation rates. For sharp concentration gradients or high scalar dissipation rates (right, Fig. 2), a narrow spatial region of flammable stoichiometry exists and the edge-flame structure is narrow. This results in high flame curvature at the base of the triple flame and reduced flow divergence around the flame. The low flow divergence also results in reduced deceleration of the flow going into the stabilization point

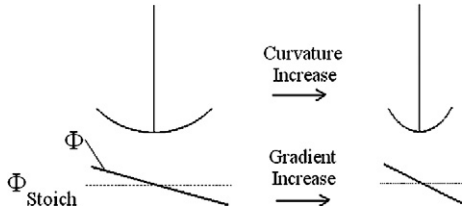

Fig. 2. The concentration gradient below each edge flame is directly proportional to the curvature at the leading edge of each flame.

and therefore a reduced overall flame propagation velocity, as reported by Dold [11]. Conversely, with a lower scalar dissipation rate (left, Fig. 2), the flammable region is expanded, resulting in a broader flame with lower flame curvature and more flow divergence. Hirota et al. [17] clearly demonstrated this strong correlation between flame curvature and the upstream concentration gradient for single edge flames. Hirota et al. [17] also found that even as the upstream velocity exiting from the burner changed, the relationship between the concentration gradient just at the flame edge and the flame curvature was unchanged.

In general, lower scalar dissipation rates lead to higher edge-flame propagation speeds, as shown by Dold [11] and Kioni et al. [6,7]. However, Kim et al. [15] showed that as the concentration gradient below the flame decreases to very small values, a critical concentration gradient exists where a minimum liftoff height or a maximum edge-flame propagation velocity is observed. Below this critical gradient, the trailing diffusion branch weakens, representing a transition from partially premixed to planar premixed propagation.

Apart from studying effects of upstream stoichiometry conditions on an edge flame, other experiments have been performed studying chemical interactions between flame branches. Azzoni et al. [16] found that neighboring edge flames could cause changes in the diffusion branch and affect propagation velocities of the overall flame structure. Counterflow studies performed by Lockett et al. [18] also examined chemical interactions between branches.

In turbulent nonpremixed flows, mixing of fuel and air by large-scale flow structures can cause numerous stoichiometry gradients [19] with multiple stoichiometric points within a few millimeters of each other, as shown by measurements of Brockhinke et al. [1] in a lifted hydrogen jet. With multiple stoichiometric crossings, the stabilization of multiple-edge-flame structures and interactions between these flames may occur; these interactions could be either chemical or aerodynamic. The work of Ghosal and Vervisch [5] presented numerical simulations in practical nonpremixed flow fields, showing complicated mixing structures that provided multiple edge-flame

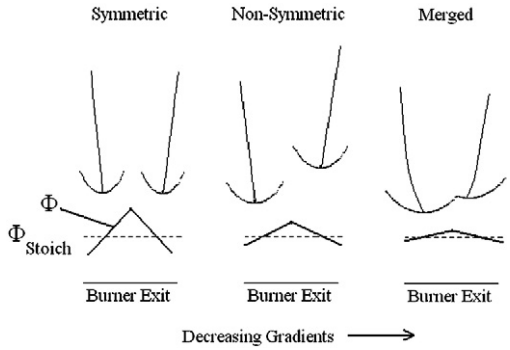

Fig. 3. Neighboring edge-flame configurations seen by Wason et al. [2] with decreasing concentration gradients from left to right.

stabilization locations. Our group [2] studied possible interactions of multiple neighboring laminar edge flames. The present work examines these interactions in detail, using optical diagnostics to probe the local mixing conditions at each stabilized flame.

Wason et al. [2] created multiple lifted edge flames using a planar slot burner, where the concentrations of five individual slots were varied to create a nonuniform concentration gradient at the exit of the burner. The use of five slots allowed two concentration gradients with two stabilization points. The previously studied flame configurations are depicted in Fig. 3, and planar images of hydroxyl in these flames are available in [2]. Under large concentration gradients (high local scalar dissipation), shown in the left panel of Fig. 3, the two neighboring edge flames stabilized at symmetric liftoff heights; however, there was an aerodynamic interaction as the flames were tilted away from the centerline of the burner. Without the neighboring edge flame, the trailing diffusion flame branch is vertical. Aerodynamic interactions here refer to changes in the flame resulting entirely from changes in the cold fuel and airflows upstream of the flame. As the concentration gradient below the flames was decreased, the individual edge flames broadened, as shown in Fig. 2, and a symmetric liftoff height was no longer maintained. One flame, denoted the upper flame in this paper, had a greater liftoff height than the lower flame. This configuration is depicted in the middle panel of Fig. 3. Further reduction of concentration gradients initially caused the liftoff height difference to increase. However, eventually the individual edge flame structures broaden sufficiently to cause the neighboring flames to attach by their rich premixed branches, as shown in the right panel of Fig. 3. Once the flames become attached to one another, the upper flame moves down toward the lower flame with a decrease in the stoichiometry gradient. A further decrease in gradient caused an approach

to premixed conditions and the flames merge into a single structure. Wason et al. [2] performed OH PLIF and PIV measurements on these flames and found that for the merged flames, OH layers were connected between flame branches, thus making possible a chemical interaction. Chemical interactions here refer to changes in the flame caused by transport of radicals and heat between individual flames. For separate flame configurations, interactions were presumed to be dominated by aerodynamics around the flames themselves. This paper focuses on a detailed study of the interactions of lifted neighboring edge flames reported by Wason et al. [2] for understanding on how interactions could affect stability of turbulent flames.

3. Specific goals

Determination of the cause of the bifurcation observed by Wason et al. [2] requires an understanding of the local conditions below and through each edge-flame structure. In particular, the flow divergence around the lower flame structure can alter the flow and mixing field for the upper flame, resulting in an aerodynamic interaction. Likewise, when the flames are merged, heat and radical transport could cause a thermal or chemical interaction altering the stability of the flame. Quantitative measurements of the scalar dissipation rates below each flame structure are important, since the local concentration gradient below a single edge flame affects the flame curvature and propagation velocity of the flame. In this paper, Rayleigh imaging was used to quantify the fuel concentration gradients directly below each flame and for extraction of flame front curvature. Flame fronts within the leading edge of each flame configuration were measured using PLIF to determine qualitative hydroxyl and formaldehyde concentrations and to estimate relative HCO formation rates based on the intensity of the combined signal [20]. Comparisons between the intensity of signals from flames were used to determine whether chemical interactions were present. Quantitative measurements of concentrations are not needed for this comparison; thus only relative fluorescence intensities without calibration were utilized. Comparisons between neighboring flames and single flames were made to determine whether aerodynamic or chemical interactions cause the flame bifurcation. The results from this work are used to suggest which parameters should be included in a detailed model of flame propagation in turbulent flows where flame interactions may be present.

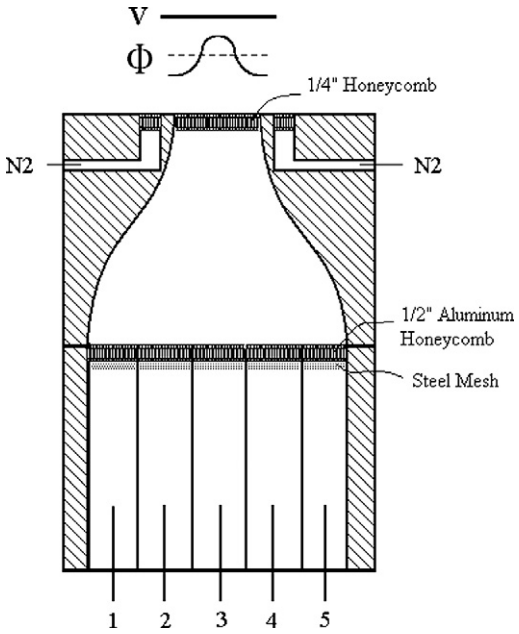

Fig. 4. Five-slot burner with contoured converging nozzle.

4. Experimental apparatus

Interacting lifted edge flames were created using a burner with five slots, as shown in Fig. 4. The burner consists of a rectangular base, which houses the inlets for each 14×120 mm slot. The slot exits contain steel wire mesh and $1/2''$-thick, $1/8''$-cell aluminum honeycomb to distribute and straighten the flow. This flow is then passed through a contoured converging nozzle, which acts to create a flat velocity profile at the exit of the burner. The contoured nozzle is 100 mm in length with an inlet cross section of 120×75 mm and an exit cross section of 25×40 mm, matching the outlet dimensions of the straight geometry burner of Wason et al. [2] and giving the burner a 3:1 convergence ratio in two dimensions.

The nozzle also acts to smooth the discrete composition gradients from the five slots. The exit of the burner contains a section of $1/4''$-thick, $1/16''$-cell steel honeycomb, which minimizes any horizontal components of velocity as the flow exits the corners of the nozzle. The honeycomb also behaves as a flame arrestor preventing flashback into the nozzle. A 5-mm-wide continuous inlet surrounding the burner exit is used for nitrogen guard flow to isolate the edge flames from the surrounding room air. The nitrogen for the guard flow was supplied through a series of rotometers to ensure uniform nitrogen delivery.

Flow for the burner was provided using electronic pressure regulators coupled with precision choked orifices. Ten regulators were connected to the burner,

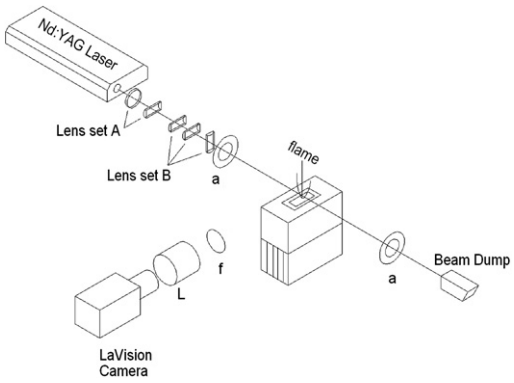

Fig. 5. Rayleigh scattering experimental setup: (l) lens, (a) aperture, (f) filter. Lens set A was used for large area 2-D Rayleigh imaging while lens set B was used for finer line measurements.

as each slot requires one for air and one for fuel. The flows were sufficiently mixed prior to entering the five-slot burner. Ethane was used as the fuel for measurements because of its higher molecular weight (compared to methane, used in [2]), close to that of air, further helping to maintain a constant velocity profile along the exit of the burner, independent of concentration profile.

Testing of edge-flame interactions was performed by using two symmetric stoichiometry gradients as in Fig. 3. The slots of the burner were set so that the ethane concentration varied from a lean, to a rich, and then back to a lean concentration across the five slots. The two outer slots, one and five in Fig. 4, were run with only air (an equivalence ratio of zero), while slots two and four were maintained at equal lean equivalence ratios. Increasing the equivalence ratio of slots two and four caused the stoichiometric crossings of the concentration profile at the exit of the burner to spread apart, as discussed within the results. The center slot, slot three, was varied from an equivalence ratio of 1.25 to 25 to vary the gradient of ethane below each flame.

Rayleigh scattering measurements were performed using a dual-cavity 50 mJ/pulse Nd:YAG laser with a 6-ns pulse width at a wavelength of 532 nm, shown in Fig. 5. For 2-D Rayleigh scattering, a laser sheet was formed using an $f = -30$ mm cylindrical lens to expand the beam and a spherical lens to focus into a sheet (Fig. 5, lens set A). This sheet was passed through the centerline of the burner and included the area underneath each of the edge flames. An iris was used to cut the lower edge of the laser sheet so that the sheet did not reflect from the burner surface during imaging. After the laser sheet passed through the flame, it was sent to a large beam dump to help reduce back reflections.

Line Rayleigh measurements were also taken to improve signal-to noise-ratios for some cases and as a comparison to the 2-D Rayleigh measurement that was performed. In this case, a much smaller laser sheet was created by not expanding the 10-mm laser output. This procedure allowed an increased signal but limited the area for which Rayleigh information was obtained. The laser sheet was formed by combining −30-, 100-, and 500-mm focal length cylindrical lenses (Fig. 5, lens set B) to narrow the width of the sheet.

A LaVision imaging system was used for the Rayleigh signal collection, including a frame-straddling 1024×1280 CCD camera (Model Flow Master 3S) and DaVis postprocessing software. A Nikon 50-mm lens was attached to the camera. A 532-nm optical pass filter was attached to the camera lens to limit collection of flame emission and background lights. Imaging was performed with on-chip integration, where 300 images were accumulated on the camera. For the line Rayleigh, where laser energy density was larger, 20 images were accumulated on the camera.

Rayleigh scattering collection was performed with an exposure time of 10 μs. In each case, additional images were taken with only nitrogen flow through the burner to measure any remaining surface scattering, and with only ethane through the burner for determining the flat field image and calibration. The nitrogen images were used as a background subtraction from both the flame image and the pure ethane image. In order to acquire a normalized image of ethane mole fraction, the background-corrected flame image was divided by the background-corrected pure ethane image. This relationship is

$$I = \frac{[\text{Signal}] - [\text{Background}]}{[\text{Ethane}] - [\text{Background}]} = \frac{[(X_{O_2})\sigma_{O_2} + (X_{N_2})\sigma_{N_2} + (X_{C_2H_6})\sigma_{C_2H_6}]}{[(1)\sigma_{C_2H_6}] - [(1)\sigma_{N_2}]} - \frac{[(1)\sigma_{N_2}]}{[(1)\sigma_{C_2H_6}] - [(1)\sigma_{N_2}]}, \quad (1)$$

where the mole fractions of the scattering species (X_i) and their scattering cross-sections (σ_i) determine the Rayleigh signal. The overall laser intensity was constant between each two measurements and cancels from this relationship. This normalization also takes into account any laser energy differences in the imaging plane. This corrected image, I, varies from zero to unity. If the scattering cross sections of nitrogen and oxygen are assumed equal, this image directly represents ethane mole fraction in the isothermal regions of the flow below each flame, as shown in

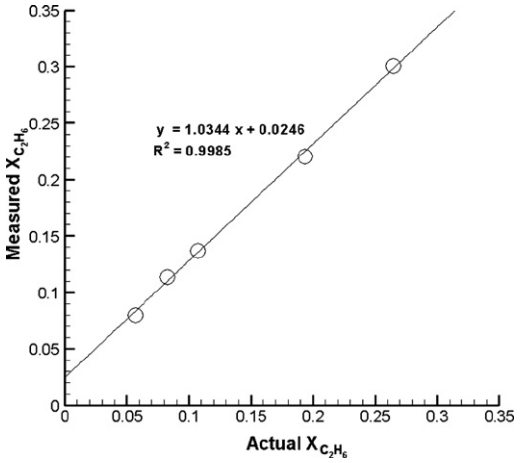

Fig. 6. Calibration for correction of normalization scheme used for Rayleigh imaging.

$$I = \frac{[(1 - X_{C_2H_6})\sigma_{N_2} + (X_{C_2H_6})\sigma_{C_2H_6}] - [(1)\sigma_{N_2}]}{[(1)\sigma_{C_2H_6}] - [(1)\sigma_{N_2}]}$$
$$= \frac{X_{C_2H_6}(\sigma_{C_2H_6} - \sigma_{N_2})}{(\sigma_{C_2H_6} - \sigma_{N_2})} = X_{C_2H_6}. \quad (2)$$

However, a small difference in the oxygen and nitrogen cross-sections actually exists, 5.245×10^{-27} cm^2 for oxygen and 5.10×10^{-27} cm^2 for nitrogen [21], causing a slight deviation in measured versus actual ethane mole fraction. A calibration of known ethane mole fraction ($X_{C_2H_6}$) in relation to the measured quantity, I, was performed in a simple laminar jet for calibration. Fig. 6 shows this calibration, which was used to provide correction for individual Rayleigh images.

PLIF imaging of hydroxyl and formaldehyde species concentrations was implemented to allow comparison between neighboring flame reaction rates. These measurements are qualitative and are only used to compare relative intensities of reaction rate between neighboring flames. The experimental setup for PLIF imaging is shown in Fig. 7. For measurements of HCHO and OH, two laser beams were passed through a plane across the exit of the burner. A Spectra Physics Pro-230-10 Nd:YAG laser with a 7-ns pulse width was used to create both beams. The doubled output at 532 nm was used to pump a Sirah Precision Scan dye laser, while the simultaneous tripled output from the Nd:YAG laser was directly used for the HCHO measurements at a wavelength of 355 nm. The pumped dye laser, containing Rhodamine 590 dye, was used for OH measurements. The dye laser was tuned to excite the $P_1(8)$ or the $P_1(4)$ transitions in the X–$A(1,0)$ vibronic band of OH at wavelengths of 285.59 and 283.47 nm, respectively. The multiplication of each fluorescence image can be used for investigation of the relative

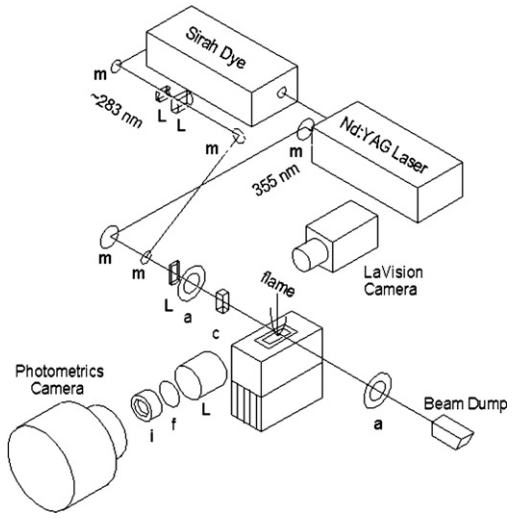

Fig. 7. Hydroxyl and formaldehyde PLIF experimental setup: (m) mirror, (l) lens, (a) aperture, (f) filter, (i) image intensifier, (c) cuvette.

forward reaction rate for $CH_2O + OH \rightarrow HCO + H_2O$ [20]. These line locations were determined through simulations of OH spectra to determine one line that was isolated with minimum temperature sensitivity, the $P_1(8)$ transition, and one line with temperature sensitivity to combine with HCHO temperature sensitivity and yield forward reaction rate [20], the $P_1(4)$ transition. Pulse energies for these beams were approximately 2.0 and 1.6 mJ for the $P_1(4)$ and the $P_1(8)$ lines, respectively. The 355-nm beam for HCHO had a pulse energy of approximately 50 mJ.

Alignment of the beams was accomplished so that each beam would pass through the same set of apertures. The beam for OH measurements from the dye laser was passed through two cylindrical lenses of focal lengths −30 and 100 mm, to increase the vertical height of the beam by a ratio of about 3. The beam for HCHO measurements was used at its laser exit height to maintain a higher energy density of the beam across the imaging plane. Both beams were passed through an $f = 500$ mm cylindrical lens to focus the beam width to a thin sheet as it crossed through the imaging area.

Imaging of all fluorescence was performed by a 1317×1035 pixel Photometrics series 300 liquid-cooled camera, Fig. 7. Fluorescence was collected through a UV-Nikkor 105-mm $f/4.5$ lens. This lens focused the fluorescence image onto a DEP-GenII image intensifier, which was gated for 1 μs at each laser pulse. This small gate was used to minimize chemiluminescence collection from the flame during imaging. The image of the intensifier was then collected by a

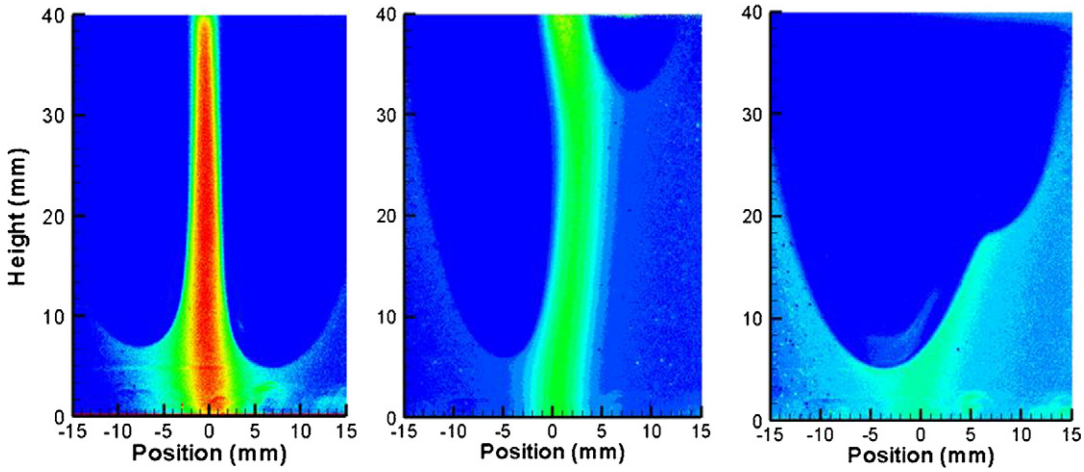

Fig. 8. Rayleigh scattering images from neighboring edge flames with changing concentration gradients below the flames.

150-mm focal length lens coupled to a Nikkor 50-mm lens attached to the Photometrics camera.

Two different optical filters were used for the fluorescence imaging. For OH measurements, a filter centered around 308 ± 5 nm was used. During the OH measurements, the 355-nm beam was blocked, and during measurements of HCHO, the 283-nm beam was blocked after exiting the dye laser. For imaging of HCHO, the OH filter was replaced by a 450 ± 40 nm band-pass filter (Omega Optical Inc. 50450 450DF70D) with approximately 70% transmission within its pass range. This range was shown to cover the broadband HCHO fluorescence when excited by a 355-nm beam [22].

The laser beam energy profiles were measured prior to each data set. For the dye laser beams, the laser was passed through a removable UV-transparent cuvette. This cuvette was filled with a linearly fluorescent solution. The fluorescence within the cuvette was imaged using the same LaVision CCD camera used for the Rayleigh scattering measurements. A Nikkor 200-mm $f/4$ UV lens was attached to the camera, which was exposed for 10 μs during each laser pulse. A 100-image average was taken for each OH beam profile. For HCHO, the beam distribution correction was measured using Rayleigh scattering from pure ethane with the 355-nm beam. A rectangular mask around the imaging area was used to minimize scatter, while the filter used for HCHO was removed to allow Rayleigh signal to pass to the intensifier.

For imaging of each flame under various flow conditions, the burner was placed on a three-axis translation stage. The location of each flame was set so that the leading edge of the flame of interest would fall at the center of the image.

5. Results and discussion

The redesigned five-slot burner, used to create a 2-D controllable concentration gradient, was tested to recreate interactions observed by Wason et al. [2] and neighboring flame behavior was found to be similar to that previously described. Three example Rayleigh images are shown in Fig. 8. For each flame, the equivalence ratio in slots 2 and 4 of the burner was fixed at 0.75, and the central slot 3 equivalence ratio was varied from 1.25 to 25. These cases represent behavior with two stoichiometric crossings, in which the concentration along the exit of the burner is that of lean to rich, then back to lean concentrations of ethane. As the equivalence ratio within slot 3 was decreased, the gradient of ethane concentration below each flame was also decreased, as shown in Fig. 3. Images in Fig. 8, from left to right, represent this decreasing equivalence ratio in the central slot of the burner. These Rayleigh images show the three stable modes depicted in Fig. 3 in which, from left to right, both flames stabilize at similar heights for symmetric conditions, one of the flames maintains a different liftoff height than that of its neighbor, and finally a merged flame in which the rich branches of both flames are connected. As with the flames described by Wason et al. [2], the flames become asymmetric immediately when lit; however, a metal rod can be used to pull the upper flame down and switch which flame edge is lower. A further description of this bifurcation is provided in [2].

The Rayleigh images from Fig. 8 can be used to measure the fuel distribution and therefore the ethane concentration gradients below the flames where the temperature is constant. In addition, the flame edge is readily apparent in the Rayleigh images as a sharp contrast in signal due to the lower density and scat-

tering within the flame. In the middle panel of Fig. 8, the fuel distribution can be clearly observed to shift to the right toward the upper flame due to the flow divergence induced by the lower flame. A primary goal of this paper is to assess if the upper flame stabilizes under the same local conditions as the lower flame and therefore to determine if the bifurcation is only a result of aerodynamic interaction or is affected by thermal interactions between flames. The Rayleigh imaging from Fig. 8 was used to determine both the ethane concentration gradient below each flame and the flame curvature of each edge flame. Extraction of the concentration gradient below each flame used a nonlinear least-squares Gaussian fit on each horizontal line below the leading edge of each flame. Fig. 9 shows a close-up of the case with $\Phi_2 = \Phi_4 = 0.75$ and $\Phi_3 = 25$, as in the left panel of Fig. 8. The stoichiometric locations are indicated by small crosses in the figure, as determined from the Rayleigh curve fits. An example of the curve fit along the line shown in Fig. 9 is shown in Fig. 10. After the Rayleigh signal was fitted along each horizontal line below all flames, the concentration gradient was determined using the analytical derivative of the fit at the stoichiometric mole fraction crossing of the fit, as shown in Fig. 10. The concentration gradients reported in the remainder of this paper were averaged over the gradients for each line between 1 and 2 mm below each flame front. This distance was found to be far enough from the flame so that no preheating of the gases had occurred, and the gradient over this distance was nearly constant, so that averaging could be used to improve signal-to-noise ratios.

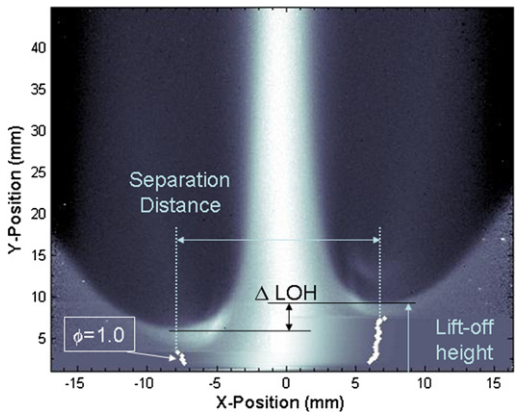

Fig. 9. Location of stoichiometric points for case with large concentration gradient below each flame.

In addition, the effect of the orientation of the gradient relative to the tilted flames was accounted for by correcting the gradient below each flame by using the angle of the stoichiometric contour at the leading edge. The angle of the stoichiometric contour was determined using position information on each stoichiometric point below the flame. A fit was made to the stoichiometric contour points and the angle at the leading edge was extracted from the fit.

The liftoff heights of both edge flames were also determined from the lowest location in the Rayleigh image, with a rapidly decreasing signal due to temperature increase. At the intersection of the stoichiometric line and the flame front, the flame curvature was determined by fitting an arc to the local region around the stabilization point. Points for the arc fit were taken along the region where the Rayleigh signal

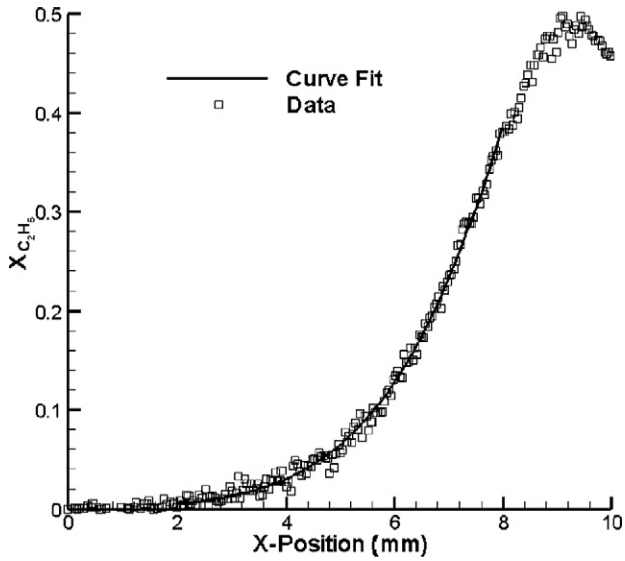

Fig. 10. Example Gaussian fit of Rayleigh data under the lower flame of a separated flame case.

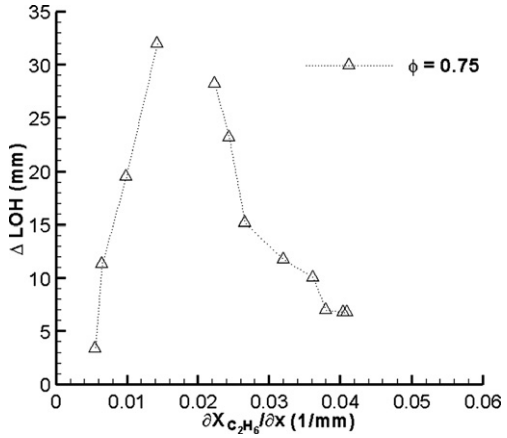

Fig. 11. Liftoff height difference versus ethane concentration gradient in neighboring edge flames.

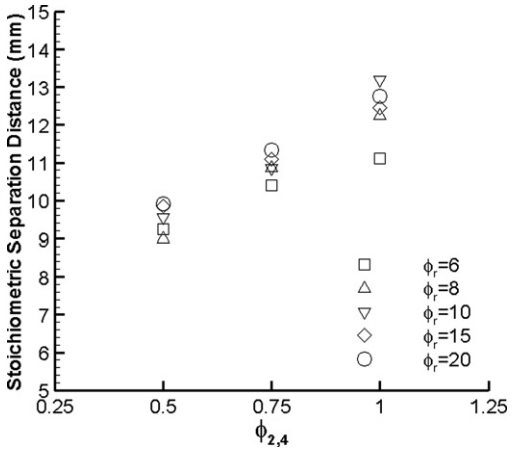

Fig. 12. Measured distance between stoichiometric points as a function of varying equivalence ratio in slots 2 and 4 of the five-slot burner.

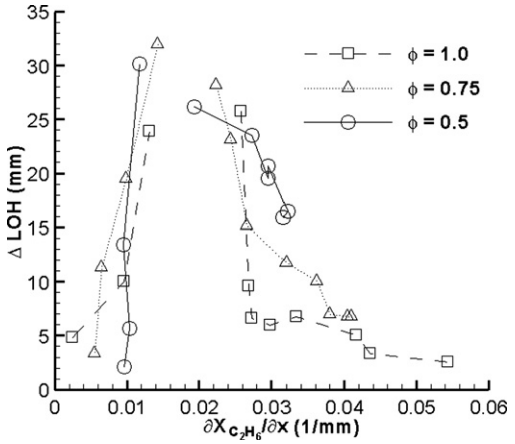

Fig. 13. Liftoff heights versus measured ethane concentration gradient 1 mm below each lower edge flame. The equivalence ratio of each data set refers to slots 2 and 4, which control stoichiometric point separation.

quickly drops due to a drop in gas density associated with a high temperature zone. The fit was performed using points spanning about 5 mm along the leading edge of each flame.

Fig. 11 shows the difference in liftoff height between the lower and upper flame (ΔLOH) versus the local ethane concentration gradient below the lower flame. As the central slot equivalence ratio is increased, the local ethane concentration gradient also increases. The flows in slots 2 and 4 were held at an equivalence ratio of 0.75 for these measurements. Starting from the far right of Fig. 11, with high central slot equivalence ratio, the two edge flames stabilize within approximately 7 mm of one another, as shown in the left panel of Fig. 8. The nonzero liftoff height difference is discussed subsequently. As the central slot equivalence ratio is decreased, the upper flame moves higher, as shown in the middle panel of Fig. 8. Once the liftoff height difference exceeds approximately 33 mm, the upper flame moves outside the field of view of the Rayleigh imaging system. On the left of Fig. 11, as the ethane fuel concentration gradient is further decreased, the upper flame begins to move back down into the field of view of the image and is now merged with the lower flame, as shown in the right image of Fig. 8. For the lowest measurable concentration gradient, with a central slot equivalence ratio of 1.25, the flames are no longer two distinct edge flames but merge into an almost single premixed edge flame. OH PLIF images showing this merger as discussed in [2].

The nonzero liftoff height difference in Fig. 11 was examined by altering the horizontal separation distance between the stoichiometric crossings on each concentration profile below the two edge flames. To change the separation distance, the equivalence ratios of slots 2 and 4 were varied and the horizontal location of the stoichiometric points was determined from the Rayleigh images as shown in Fig. 11. Fig. 12 shows the stoichiometric separation distance for equivalence ratios in slots 2 and 4 of 0.5, 0.75, and 1.0, with a changing equivalence ratio in the center slot (ϕ_r). By increasing the slot 2 and 4 equivalence ratios, the horizontal separation distance between flames can be increased by as much as 4 mm.

Fig. 13 shows measured liftoff height differences between the upper and lower flame branch versus measured ethane mole fraction gradients below the lower flame branch for three sets of data with different equivalence ratio values in slots 2 and 4. The $\Phi_{2,4} = 0.75$ data are repeated from Fig. 11. With an equivalence ratio of 0.5 in slots 2 and 4, separated edge flames occur for gradients below the lower flame above 0.015 mm^{-1}. For shallower gradients, a

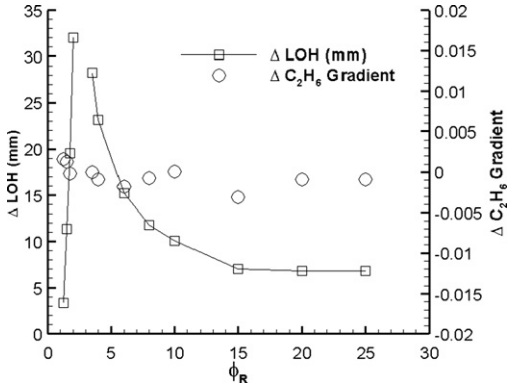

Fig. 14. Difference between concentration gradients below neighboring edge flames and liftoff height difference versus the central slot equivalence ratio.

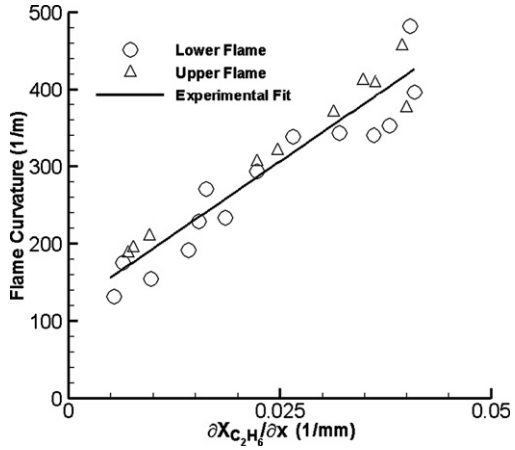

Fig. 15. Correlation between flame curvature and local leading edge concentration gradient for all stability configurations.

merged flame structure is observed. For very rich center slot flows with higher gradients below the lower flame, the liftoff height difference levels off to a value of about 16 mm. The difference in liftoff height reaches this minimum value and does not decrease with richer flow in the center slot.

Increasing the separation distance between the stoichiometric points by increasing the equivalence ratio of slots 2 and 4 to 0.75 resulted in a similar overall trend in the liftoff difference between flames. The transition from a merged flame structure to a separated flame structure occurred at similar concentration gradients. Moreover, the difference between liftoff heights at high fuel concentration gradients approached 7 mm as the equivalence ratio was increased in the center slot. For equivalence ratios in slots 2 and 4 of 1.0, thus further separating the stoichiometric points below the flames, the difference in liftoff heights with large local gradients is only 3 mm. The width of each individual edge flame increases as the stoichiometry gradient below the flame decreases (Fig. 2). For narrow edge flames, the interactions are diminished and nearly symmetric flames are achieved (right of Fig. 13). However, the width of the edge-flame structure that causes interactions is relative to the distance between edge-flame stabilization locations. For smaller horizontal separation distances, larger interactions are observed, while for larger separation distances, the flames can become completely symmetric. The transition from merged to separate flames for each case occurred at a similar concentration gradient of about 0.015 mm^{-1}.

Figs. 11 and 13 are each plotted against only the lower flame's local concentration gradient. The Rayleigh images were also used to extract the concentration gradient below the upper flame for comparison. Fig. 14 shows the difference in ethane mole fraction gradient between the lower and neighboring upper flame,

$$\Delta \text{C}_2\text{H}_6 \text{ gradient} = \left.\frac{\partial X_{\text{C}_2\text{H}_6}}{\partial x}\right|_{\text{upper}} - \left.\frac{\partial X_{\text{C}_2\text{H}_6}}{\partial x}\right|_{\text{lower}}, \tag{3}$$

versus the central slot equivalence ratio. When the flames are merged together, there is a slight scatter in the difference between the concentration gradients below each flame; this scatter takes place around a value of zero. For a central equivalence ratio greater than 5.0, when the flames are separated, there is no discernible difference in the concentration gradient below the neighboring flames. This zero difference suggests that the upper flame's stabilization is identical to that of the lower flame and that the dominant interaction causing a liftoff height difference is purely due to changes in the upstream flowfield for the upper flame due to flow divergence around the lower flame (aerodynamic interaction).

Hirota et al. [17] showed for single edge flames that the local flame curvature was linearly related to the local fuel concentration gradient, independent of other experimental conditions such as overall flow velocity. A similar analysis of interacting edge flames is shown here, where the Rayleigh images were used to determine curvature of the upper and lower flames. The flame curvature was extracted at the stoichiometric streamline crossing point of the leading edge of each flame. Fig. 15 shows local curvature versus ethane gradient for both upper and lower neighboring flames irrespective of the configuration of the flames; i.e., both merged (below approximately 0.015 mm^{-1}) and separated flames are included in the figure. A nearly linear relationship between these quantities is present as in [17]. The common correlation of all flames suggests that each flame, whether it

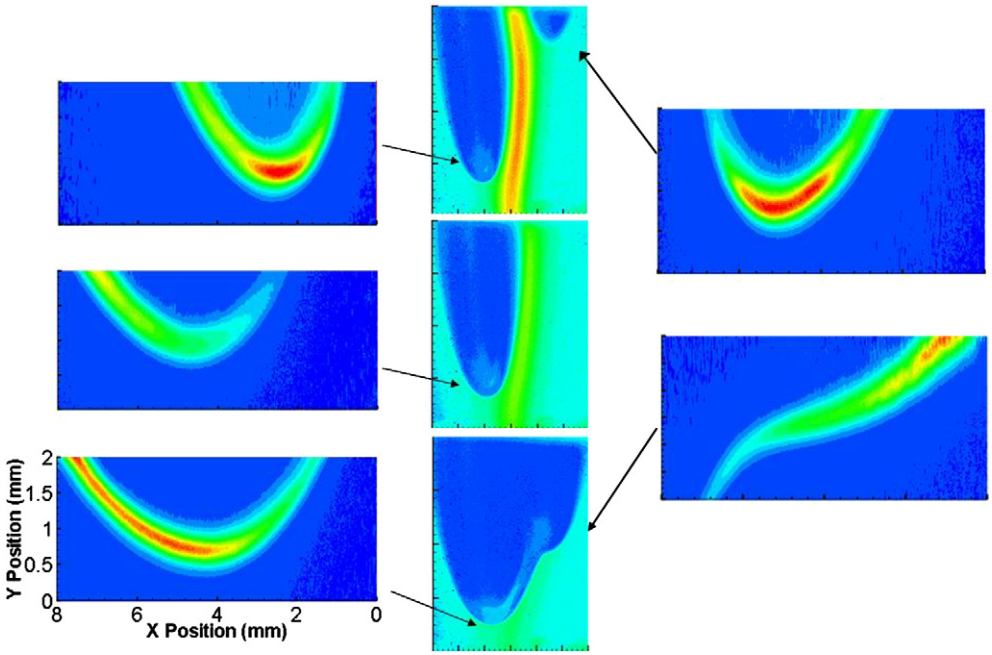

Fig. 16. Relative heat release zones of neighboring edge flames under various ethane concentration gradients. Contours are determined from the multiplication of OH and HCHO fluorescence intensity, which correlate to qualitative HCO production rate. Rayleigh images for the flame configurations are shown in the middle.

is at a greater liftoff height, separate or merged, is behaving as though it was a single flame based solely on the local conditions upstream of its flame edge.

Thus far, evidence has been given suggesting that flame interactions have been dominantly aerodynamically driven; however, to further examine the possibilities of aerodynamic and chemical effects on the interaction between these neighboring edge flames, a relative reaction rate comparison of neighboring flames was made. PLIF imaging of OH and HCHO was performed and together these PLIF images were used to determine the qualitative heat-release zone at the leading edge of each flame. The PLIF images were not calibrated as to concentration and no reaction rate premultiplier was used to determine these relative reaction rates. However, the temperature dependence of the reaction rate and its distribution should be qualitatively captured by these fluorescence intensity measurements. Fig. 16 shows the multiplication of OH and HCHO fluorescence images to produce a qualitative reaction rate contour for both upper (right) and lower (left) flame edges. The three sets of data comprise several flame configurations including separated flames with high local fuel gradients (top), separated flames with the upper flame out of the image (middle), and merged flames (bottom).

For separated flames, the maximum relative reaction rate zone (presumed to correlate with maximum heat release) occurs at the leading edges of both the upper and lower flames. This region also occurs at the same location as the stoichiometric streamline determined from Fig. 9. However, as the flames interact more strongly, the peak heat release moves away from the leading edge of the flame. The stoichiometric streamlines for these cases also show that the intersection of the stoichiometric line and the flame edge is pushed outward toward the lean side of the flame and corresponds to the same location as the peak reaction rate. It appears that the interactions between the edge flames push the stoichiometric points outward so that the stabilization points do not occur at the lowest leading edge of the flame.

Heat release profiles through neighboring flames are compared in Figs. 17 and 18. For separated edge flames, the relative reactions rate profiles show identical behavior with the same width and maximum reaction rate. Note that the PLIF imaging approach to estimating this reaction rate is not quantitative in that no calibration for absolute reaction rate was performed, but relative comparisons between flames are independent of these calibrations. For the merged flames, shown in Fig. 18, that maximum values of relative heat release appear to differ by almost a factor of 2. However, the cause for this difference is believed to result from a small unsteadiness of the upper flame, when the flames are merged. Single-shot images of the OH distribution in the upper flame show a small 1-mm oscillation in the liftoff height,

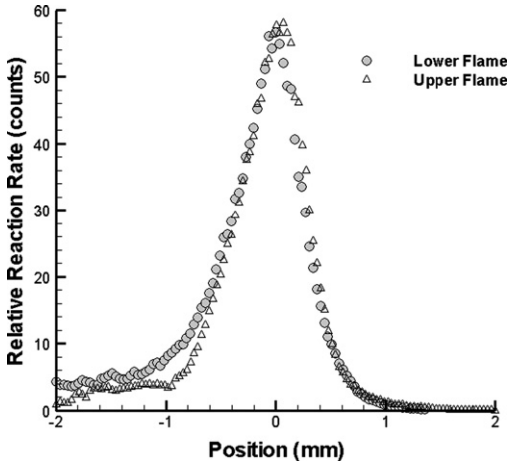

Fig. 17. Relative reaction rate profiles across flame edge at stoichiometric points of flame for separate-symmetric-flames configuration.

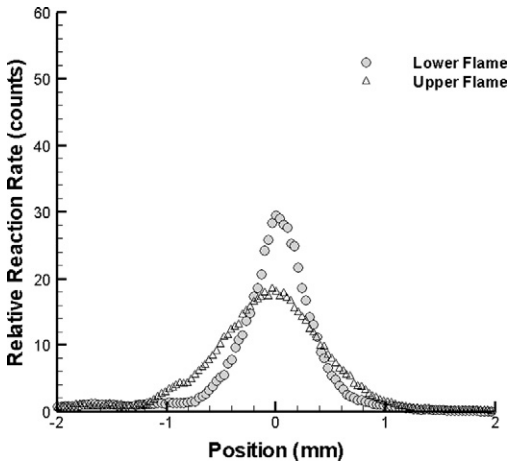

Fig. 18. Relative reaction rate profiles across flame edge at stoichiometric points of flame for merged-flames configuration.

which will broaden the region of heat release measured using averaged PLIF images and at the same time lower the maximum value. To compare the reaction zone intensities of these merged flames the area below these cross-sections was integrated to obtain a total reaction rate value. The areas were found to be 21.87 counts × mm and 21.79 counts × mm for the lower and upper flame, respectively. These values indicate that even for the merged flames, the total reaction rate intensities are within 1% of each other, and the 1-mm positional oscillation is likely the only cause for the difference of Fig. 18.

Flame interactions have been shown to be dominated by aerodynamic effects below the flame edges, and there is a critical gradient for the transition between merged flames and separate flames. This critical gradient can be physically understood by examining the flame curvatures and separation distances as shown in Fig. 19. A parameter, ψ, can be computed that relates the combined flame curvatures (related to flame widths) to the stoichiometric separation distance between the flames as

$$\psi = \frac{\rho_1 + \rho_2}{\delta_{\text{stoich}}}, \tag{4}$$

where ρ_i is the radius of curvature at the leading edge of the neighboring flame of interest and δ_{stoich} is the stoichiometric separation distance. ψ indicates when two neighboring flames would begin to overlap based on their curvatures and the distance between them. Fig. 20 shows the computed values of ψ compared to changes in liftoff height between each of the flames in this study. The transition between merged and separate flames takes place around $\psi = 1$. As ψ goes to zero, there is no interaction between flames, as the stoichiometric separation distance is large relative to the flame curvatures. For $\psi > 1$, a merged flame configuration occurs, and for $\psi \gg 1$ the con-

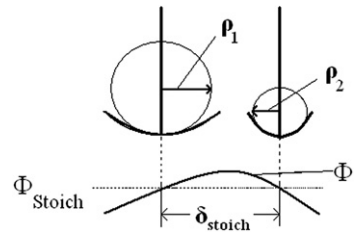

Fig. 19. Schematic of flame interactions based on flame curvature and stoichiometric separation distance.

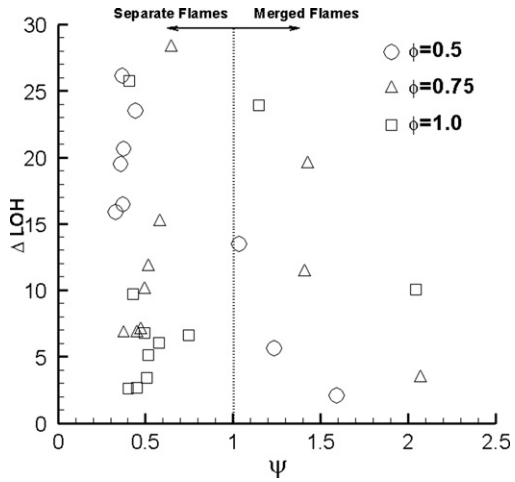

Fig. 20. Relationship between ψ and ΔLOH for all flame cases studied. A transition between merged and separate flames occurs near $\psi = 1$.

centration gradient below the flames is smoothed and approaches premixed conditions.

For the flames in this study, the upper and lower flame stabilize at the same concentration gradient and therefore similar flame curvature (see Fig. 15). Thus, under these symmetric conditions, Eq. (4) reduces to

$$\psi \approx \frac{2\rho}{\delta_{\text{stoich}}}. \tag{5}$$

Therefore, the value of ψ approaches 1 when the radius of curvature of the flames approaches half of the stoichiometric separation distance. For the case of the experiments performed in this paper, the stoichiometric separation distance was ≈10 mm (Fig. 12); therefore the critical radius of curvature would be about 5 mm. Fig. 15 shows that this curvature ($1/5$ mm $=$ 200 m^{-1}) occurs near a concentration gradient of 0.015 mm^{-1}.

6. Conclusions

Neighboring edge-flame interactions were created using a five-slot burner, modified from previous work, in which flow velocity was kept constant using a contoured nozzle and the fuel concentration profile was varied to create multiple stoichiometric crossings in close proximity. The liftoff characteristics of the neighboring flames were similar to that found by Wason et al. [2]. In particular, for large stoichiometry gradients and large separation distances, the neighboring edge flames stabilize at similar liftoff heights and show minimal interaction. When the stoichiometry gradient below the lifted edge flames is decreased, one neighboring flame's liftoff height increases. Eventually, with further decreasing stoichiometry gradients, the two edge flames merge and the liftoff height difference begins to decrease. Further reduction of the stoichiometry gradients results in the two edge flames merging until the flames appear to be a single premixed flame. It was observed that as the separation distance between interacting flames increases, the liftoff height difference decreases. Symmetric liftoff height conditions can exist, but the separation distance between neighboring flames must be sufficiently large relative to the width of the individual flames.

Flame interactions were observed while changing the stoichiometric separation distance and concentration gradient below the two neighboring edge flames. Rayleigh scattering measurements were used to determine the concentration gradients and flame curvature. A correlation between these values showed that neighboring edge flames behaved as single flames based upon local upstream conditions. OH and HCHO PLIF measurements were used to determine the relative intensity and location of the heat release zone of each flame. Qualitative reaction rates of neighboring edge flames were found to be similar, independent of the configuration of the flames, also suggesting that minimal chemical interaction was present between flames. Thus, only aerodynamic interactions were observed for all cases examined.

A critical fuel mole fraction gradient of about 0.015 mm^{-1} was found to define the transition from merged to separate flames for all experimental cases. If the radius of curvature of the two flames in sum is greater than the stoichiometric separation distance below the neighboring flames, the flames will merge and decreasing fuel concentration gradients will cause the liftoff height difference to decrease. When the flame curvatures add to less than the separation distance, the flames remain separated and decreasing fuel concentration gradients below the flames lead to increasing liftoff height differences.

For large stoichiometry gradients (high scalar dissipation rates), neighboring triple flames are narrow and do not significantly alter the flow upstream of neighboring flames. However, as the gradient is decreased, the flames broaden and the divergence of flow around a single edge flame causes an increase in the scalar dissipation rate on nearby streamlines. These steeper local gradients cannot initially support the stabilization of a second edge-flame structure, requiring additional mixing times resulting in the observed liftoff height differences. As the flames continue to broaden, past the critical gradient related to the flame curvatures and separation distances, the flames merge. Modeling of lifted flame stabilization or edge flame propagation in a turbulent nonpremixed flow where stoichiometry gradients will exist over a range of scales can include these interactions by consideration of the local conditions in the isothermal regions of the flow. Single edge-flame studies that characterize the propagation velocity and curvature of an edge flame versus the scalar dissipation rate provide sufficient information for describing multiple edge-flame propagation provided that the local mixture gradient conditions are correctly described.

Acknowledgments

The authors thank Nathan Hemming and Thomas J. Mealy, of the University of Connecticut, for fabrication of the burner used for experimentation. This work was funded by the National Science Foundation (CTS#0235114).

References

[1] A. Brockhinke, S. Haufe, K. Kohse-Höinghaus, Combust. Flame 121 (2000) 367–377.

[2] A. Wason, W.F. Carnell Jr., M.W. Renfro, Combust. Sci. Technol. 178 (2006) 789–811.

[3] P.H. Paul, H.N. Najm, Proc. Combust. Inst. 27 (1998) 43–50.

[4] H. Philips, Proc. Combust. Inst. 10 (1965) 1277.

[5] S. Ghosal, L. Vervisch, J. Fluid Mech. 415 (2000) 227–260.

[6] P.N. Kioni, B. Rogg, K.N.C. Bray, A. Linan, Combust. Flame 95 (1993) 276.

[7] P.N. Kioni, K.N.C. Bray, D.A. Greenhalgh, B. Rogg, Combust. Flame 116 (1999) 192–206.

[8] V.S. Santoro, A. Linan, A. Gomez, Proc. Combust. Inst. 28 (2000) 2039.

[9] N.I. Kim, J.I. Seo, Y.G. Guahk, H.D. Shin, Combust. Flame 146 (2006) 168–179.

[10] A. Linan, A. Crespo, Combust. Sci. Technol. 14 (1976) 95.

[11] J.W. Dold, Combust. Flame 76 (1989) 71–88.

[12] L.J. Hartley, J.W. Dold, Combust. Sci. Technol. 80 (1991) 23.

[13] J. Daou, A. Linan, Combust. Theory Model. 2 (1998) 449.

[14] G. Ruetsch, L. Vervisch, A. Linan, Phys. Fluids 6 (1995) 1447–1454.

[15] N.A. Kim, J.L. Seo, K.C. Oh, H.D. Shin, Proc. Combust. Inst. 30 (2005) 367–374.

[16] R. Azzoni, S. Ratti, S.K. Aggarwal, I.K. Puri, Combust. Flame 119 (1999) 23–40.

[17] M. Hirota, T. Yokomori, K. Yasuda, Y. Nagai, M. Mizomoto, G. Masuya, Proc. Combust. Inst. 31 (2007) 893–899.

[18] R.D. Lockett, B. Boulanger, S.C. Harding, D.A. Greenhalgh, Combust. Flame 119 (1999) 109–120.

[19] L. Muniz, M.G. Mungal, Combust. Flame 111 (1997) 16–30.

[20] B.O. Ayoola, R. Balachandran, J.H. Frank, E. Mastorakos, C.F. Kaminski, Combust. Flame 144 (2006) 1–16.

[21] M. Sneeps, W. Ubachs, J. Quant. Spectrosc. 92 (2005) 293–310.

[22] T. Metz, X. Bai, F. Ossler, M. Aldén, Spectrochim. Acta Part A 60 (2004) 1043–1053.